Proceedings World Geothermal Congress 2015
Melbourne, Australia, 19-25 April 2015

A Supercritical Model of the Menengai Geothermal System

John O'Sullivan[1*], Ezekiel Kipyego[2], Adrian Croucher[1], Cornel Ofwona[2] and Mike O'Sullivan[1]

[1]Department of Engineering Science, University of Auckland

[2]Geothermal Development Company, Nairobi, Kenya

*jp.osullivan@auckland.ac.nz

Keywords: Numerical Reservoir Modelling, Menengai, Supercritical, TOUGH2

ABSTRACT

The Menengai geothermal system is hosted in a ring-like caldera a short distance north of the city of Nakuru in Kenya. In 2010 it became the second field in Kenya to be developed for energy generation, following Olkaria, which has proven to be successful and is currently undergoing expansion. In 2013 a preliminary numerical model of the Menengai field was developed (Kipyego *et al.*, 2013) which highlighted the structural control of the system and provided initial insights into its behaviour. The model also demonstrated that the standard TOUGH2 simulator was not sufficient for modelling the supercritical conditions known to exist at depths below 3200m.

In this work a new model is developed in which supercritical conditions are imposed in the upflow region of the bottom boundary. The model is run using the University of Auckland supercritical version of the TOUGH2 simulator (Croucher and O'Sullivan, 2008) with the air-water equation of state.

Comparisons of modelled downhole temperatures with field data show that the supercritical model achieves a significantly better match than the preliminary model and that artificially low permeabilities are not required at the bottom of the model to replicate the high temperatures encountered. The possible production and reinjection scenarios investigated previously are implemented using the supercritical model and the differences discussed.

1. INTRODUCTION

Located in the Great Rift Valley in Kenya, Menengai Crater is a massive shield volcano with one of the largest calderas in the world. Leat (1984) describes the caldera as a major topographical feature of Great Rift Valley and the best preserved Krakatau-style caldera in the world. Following Olkaria, the geothermal field hosted within the caldera is the second in Kenya to be investigated for development, with surface exploration beginning in 2004 (Kipyego *et al.*, 2013). Since 2011 a number of exploration wells and production wells have been drilled with maximum temperatures recorded in excess of 390°C, demonstrating the potential of the field for energy production. The location of the Menengai system is shown in Figure 1.

Previously we proposed a conceptual model of the Menengai system, used it to develop a numerical model and ran a number of scenarios (Kipyego *et al.*, 2013). The model was developed using AUTOUGH2 (Yeh *et al.*, 2012), the University of Auckland version of the TOUGH2 simulator (Pruess *et al.*, 1999) with the equation of state for a mixture of air, water and steam (EOS3).

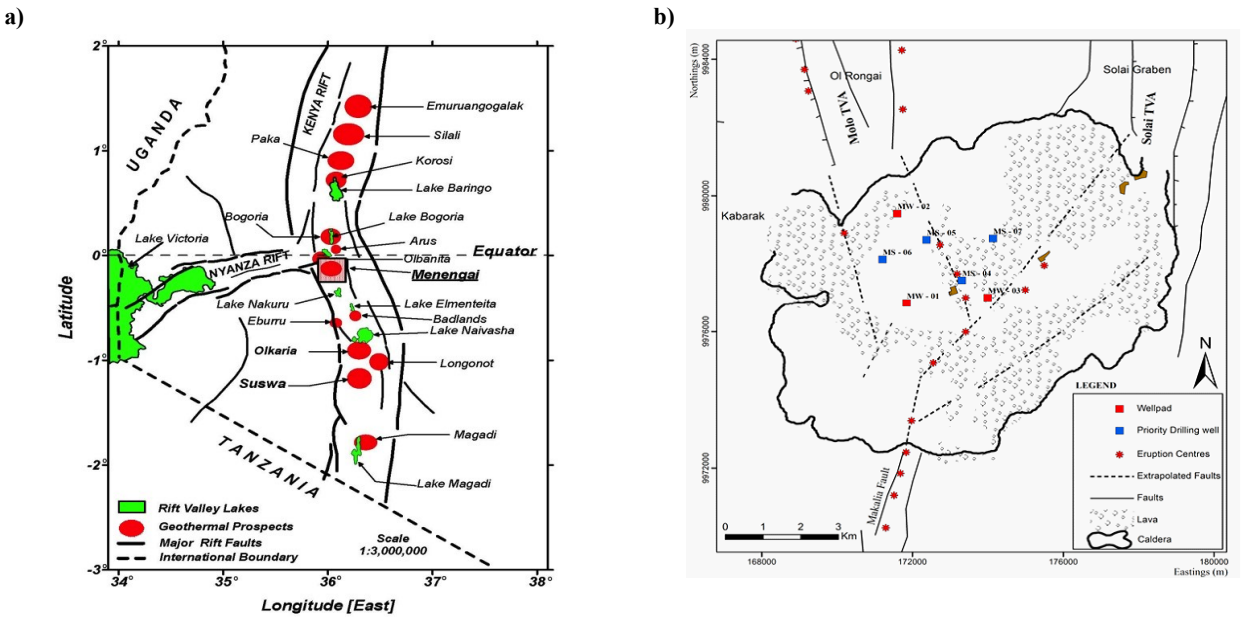

Figure 1: (a) Location of the Menengai geothermal field at the triple junction of the Nyanza Rift and the Great Rift Valley (adapted from Simiyu, 2009). Map of the Menengai geothermal field (b) with the structural geology indicated (source: Mibei and Lagat, 2011).

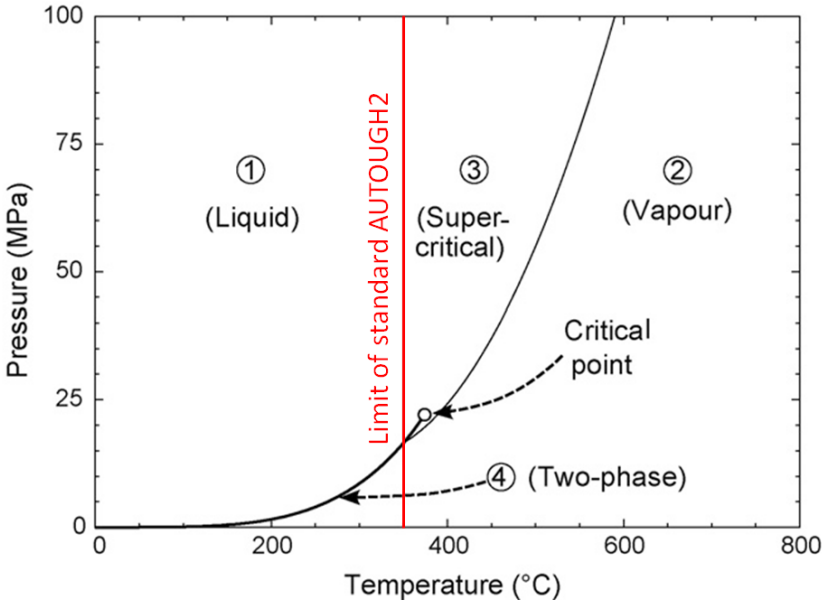

Figure 2: Temperature–pressure diagram for the IAPWS-97 pure water thermodynamic formulation. The limit of the standard TOUGH2 code is indicated by a red line (adapted from Croucher and O'Sullivan, 2008).

While the model proved to be a useful tool for increasing our understanding of the Menengai system, its accuracy was compromised because of the limitations of the standard AUTOUGH2 simulator. Figure 2 shows the temperature-pressure diagram for pure water with the maximum temperature at which AUTOUGH2 can operate accurately indicated by the red line. From the downhole measurements already recorded it is clear that fluid at temperatures well above 350°C is present in the Menengai system at relatively shallow depths (~2000 m below the surface). To overcome this limitation we were forced to lower permeabilities and reduce heat flows to ensure that conditions remained within the operating limits of standard AUTOUGH2 (Kipyego *et al.*, 2013). At the time we documented the shortcomings of the model and suggested that the supercritical version of AUTOUGH2 (Croucher and O'Sullivan, 2008) be used to develop a more accurate model of the system.

This paper presents the new supercritical version of the Menengai model, discusses its development and compares results from a number of scenarios with those from the standard version of AUTOUGH2.

2. MODEL DESIGN

The numerical model of the Menengai system was designed using the standard practice described by O'Sullivan *et al.* (2001). A conceptual model was developed using all the available information and this was used to determine the appropriate size, extent and location of the numerical model. The representative model geology was assigned and boundary conditions were imposed at the top and bottom of the model. Each of these is discussed in detail in the following subsections.

2.1 Conceptual Model

The conceptual model of the Menengai system has been described previously (Kipyego *et al.*, 2013) and is only summarised here for completeness.

- Borehole geology indicates that the subsurface stratigraphic structure of the Menengai caldera consists of three main rock units, inherited from the evolution history of the caldera.
- An upflow of high temperature fluid (above 300°C) arises beneath the Menengai caldera through buried structures and is manifested at the surface by fumaroles.
- The geochemical analysis of the fumarolic gas indicates a deep, high temperature reservoir.
- Two separate boiling zones at elevations between 1000 to 1500 masl and 400 to 700 masl were identified from hydrothermal alteration of minerals occurring there.
- The heat source for the system is a shallow magma chamber with a hot intrusive penetrating into the reservoir (Lagat, 2011).
- Recharge of cold water is from the east and northeast of the geothermal field and is controlled by major faults trending NW-SE along the minor axis of the caldera (Leat, 1984), the caldera wall and other minor structures in the caldera.
- Both complex subsurface fractures and lithologic contacts provide the permeability controlling recharge and upflow.
- Probable fluid flows in the NW, W and NE directions from the upflow region, forming the outflow of the Menengai reservoir, have been inferred by the presence of hot shallow boreholes in these regions (McCall, 1967; Wheildon *et al.*, 1994).
- Resistivity information shows that the geothermal reservoir also extends from the centre of the caldera towards the northwest as far as the Olrongai ridge

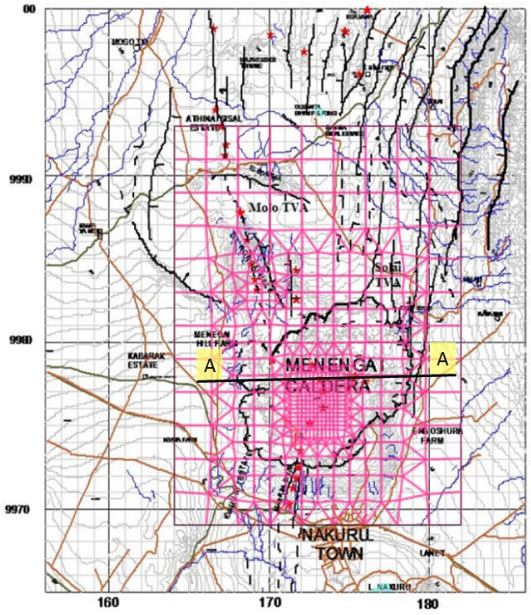

Model Area	**18 km x 24 km**
Model Depth	**3.2 km**
Number of blocks	**8391**
Number of layers	**17**
Minimum block area	**250 m x 250 m**
Minimum layer thickness	**100 m**
Rainfall rate	**1050 mm/year**
Infiltration rate	**3%**

Figure 3: Model grid design overlaid on a map of the Menengai caldera and the surrounding area. Section A-A indicated for subsequent figures.

2.2 Model Extent, Location and Grid Structure

The grid used for the supercritical model was the same as that used previously for the standard model. It includes a volume 24 km long by 18 km wide and 3.2 km deep. The model was positioned so that the entire caldera was covered with at least a 2 km buffer between the caldera wall and the edge of the model. The surface area of the model was considered large enough to capture the meteoric recharge for the system. In the north, the domain was extended so that the model covered the Olrongai ridge and the Barina swamp where the water table reaches the surface.

A total of 8391 blocks distributed over 17 vertical layers make up the model grid. The top of the model follows the topography of the area by adjusting the thicknesses of the top blocks and omitting them where necessary. The layer thickness ranges from 100 m to 500 m and the model extends from an elevation of 2200 masl to -1000 masl. At the edges of the model, the grid blocks are 2km by 2km but two levels of local refinement were used to create a higher resolution grid in the areas of most interest. This results in a resolution of 250 m by 250 m in the current drilling area in the centre of the caldera. The grid is overlaid on a map of the Menengai caldera and surrounding area in Figure 3.

2.3 Model Geology

The objective of this work was to compare the results obtained using the supercritical version of AUTOUGH2 with those obtained using the standard version. In order to make a quantitative comparison the model geology used in this work was the same as that used previously (Kipyego *et al.*, 2013). This means that locations of model rock types were the same within both models but that the permeabilities of some rock types differed between the models as a result of the calibration process. The standard model was designed to explicitly represent the major geological formations and structures to a satisfactory level while still maintaining a relatively coarse model, to allow for rapid model development. A simplifying assumption was made was that the geological formations were in horizontal layers as determined by the available well geology reports (Omondi, 2011; Mibei and Lagat, 2011). Seven major composite rock units were defined and allocated to the layer structures of the model as shown in Figure 4.

The structures included in both models were the Molo TVA, the Solai TVA, Makalia fault, the caldera wall and an extension of the Molo TVA fault into caldera. The caldera was divided into two, separating exploration wells that are hot in the shallow zone in the SW from those that are colder in the NW. Each of these two halves was then divided further into an inner and outer zone. Within each layer the model rock-type assigned to a given block was based on these structures, thus assuming that the parts of the formation located along a fault or within the caldera have undergone different stress regimes, leading to different rock properties. The rock-type assignment for a single layer with each structural zone indicated is shown in Figure 5.

In total the vertical and horizontal rock structure combine to give 93 model rock types. Details of the rock properties used for the different rock types have been given previously in Kipyego *et al.* (2013).

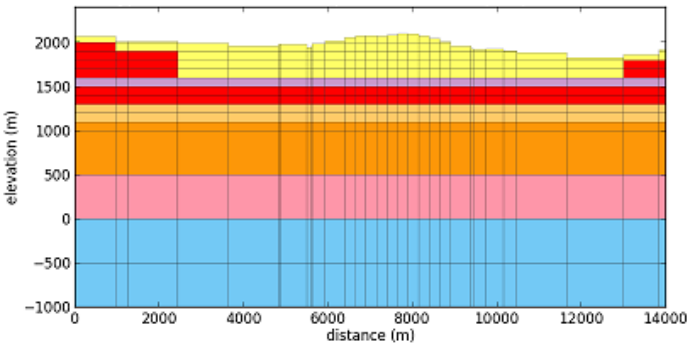

	Rock Type	Model prefix
	Predominantly pyroclastics	TS
	Trachytic tuff	TU
	Trachyte	T0
	Predominantly rhyolite	RH
	Mixture of trachyte and trachy-phonolites	T1
	Predominantly basalt and syenite	BA
	Predominantly trachyte	T2

Figure 4: Vertical rock structure in the model on section A-A.

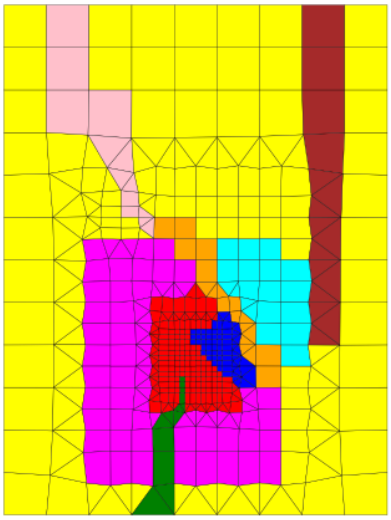

	Structural zone	Model suffix
	Caldera hotter inner zone	CHI
	Caldera colder inner zone	CCI
	Caldera hotter outer zone	CCO
	Caldera colder outer zone	CHO
	Solai TVA	F1
	Molo TVA	F2
	Molo TVA caldera extension	F3
	Makalia fault	F4
	Outer zone	OUT

Figure 5: Horizontal rock structure in the model representing major faults and caldera structures.

2.4 Boundary Conditions

The boundary conditions applied to the standard model and the supercritical model were the same at the top surface and side boundaries. At the bottom of the model they differed significantly. Each of the boundary conditions is described in the following subsections.

2.4.1 Top Surface

In both models the atmospheric layer was set to contain air at standard atmospheric pressure and a constant temperature of 20°C. The meteoric recharge by rainwater at the surface was approximated by injecting water with an enthalpy of 83.9 kJ/kg (corresponding to 20°C) into the top layers of the models. The injection rate was calculated to correspond to an annual average rainfall of 1050 mm/yr with an infiltration rate of 3%. Water at 20°C was also injected into the surface block corresponding to the point where the Bahati stream enters the caldera and disappears into the subsurface. The same estimated flow rate of 100 l/s was used to represent the stream as in our previous work.

2.4.2 Side Boundaries

All side boundaries of both models were set to be closed, thus enforcing no flow across them. This is an approximation of the real system and is one of the motivations for placing the model boundaries as far from the reservoir as computational cost will allow (O'Sullivan *et al.*, 2001). For the Menengai system ground water flow is from south to north from the caldera to the Barina swamp and beyond. To represent this in both models deliverability wells (Pruess *et al.*, 1999) were assigned in the blocks along their northern edges down to a depth of 300m below the surface. These wells allow groundwater to flow out of the models as required to maintain a hydrostatic pressure gradient.

2.4.3 Bottom Boundaries

As described in Section 2.2 the grid structure was refined in the upflow zones identified by Simiyu (2009) at the Menengai caldera and the Olrongai volcano. In both models additional heat above the background level of 0.07 W/m^2 was applied in these areas at the bottom boundary. For the standard model the additional heat flux that could be applied was restricted by the maximum temperature

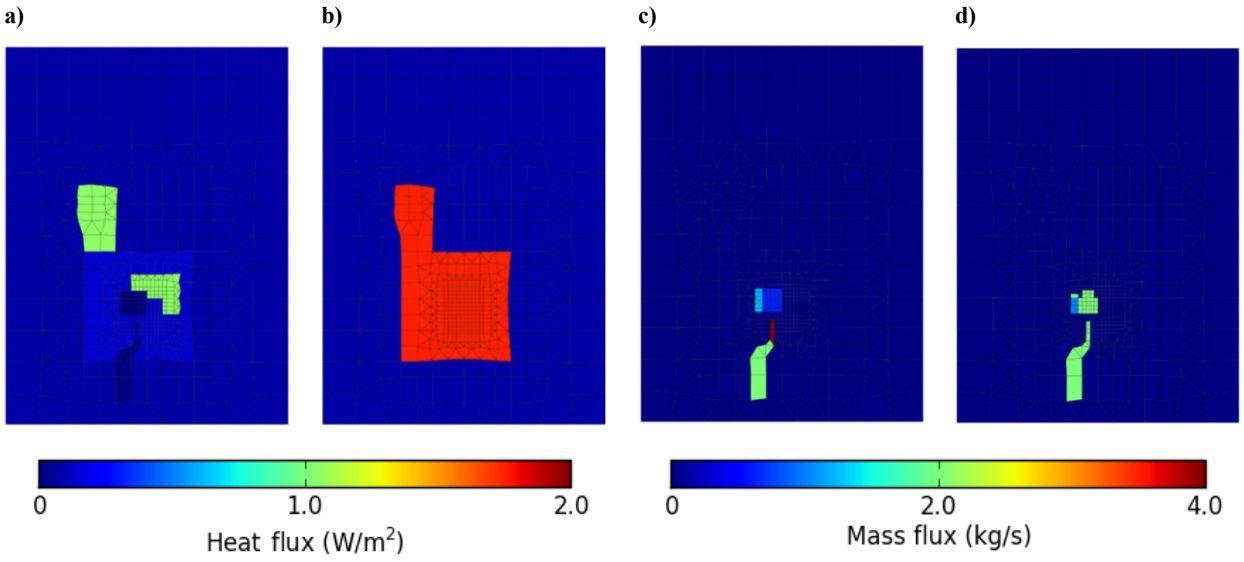

Figure 6: Heat flux boundary conditions at the bottom of the (a) standard model and (b) supercritical model. Mass flux boundary at the bottom of the (c) standard model and (d) supercritical model.

limitations. As a result maximum values of 1.05 W/m^2 were applied under Olrongai volcano and the NE section of the caldera with less applied elsewhere. The heat flux applied at the bottom boundary of the best-fit supercritical model was both greater in magnitude at 1.75 W/m^2 and more widely distributed. The bottom boundary conditions for both models are shown in Figure 6.

Plots (c) and (d) show that the mass flux boundary condition is similar for both best-fit models. The supercritical model has a slightly more even distribution and the total is slightly lower at 80 kg/s compared to 100 kg/s for the standard model. The mass flux input represents the hot deep upflow that comes from beneath the bottom of the model domain. In the case of the standard model an enthalpy of 1670 kJ/kg was used, corresponding to liquid water at 350^{o}C. This value is less than that recorded at the bottom of the exploration wells but is within the temperature limitations of the standard AUTOUGH2 code. For the supercritical model the best fit to the measured downhole temperatures was achieved using an enthalpy of 2900 kJ/kg which corresponds to water at supercritical conditions with a temperature of approximately 425^{o}C.

4. NATURAL STATE MODEL RESULTS

The supercritical natural state model was calibrated by starting with the model properties from the best-fit standard model, then slowly increasing the heat flux at the bottom of the model. As the temperatures increased, the permeabilities of several rock-types were adjusted to maintain the inflows and outflows observed in several of the downhole temperature profiles. Many iterations of this process were required to obtain the best-fit supercritical model presented here.

The results for downhole temperatures produced by the best-fit standard model and the best-fit supercritical model are shown in Figure 7. In each plot a diagram of the caldera indicates the location of the well with a red point. For more detailed information about the wells refer to Kipyego *et al.*, (2013).

Plot (a) of Figure 7 shows that both models match the downhole temperatures in MW-01 reasonably well. The cold inflow in the shallow zone is not captured by either model but the slight cold inflow at ~250 masl is represented. The high temperatures at the bottom of the well are not predicted by the standard model due to the limitations of the standard AUTOUGH2 code. The supercritical model improves on the standard model and predicts the temperatures well but is unable to match the very steep temperature gradient encountered. To capture this gradient and to improve the match in the shallow zone a higher level of refinement in the supercritical model will be required.

For MW-03 the supercritical model provides a significant improvement over the standard model. The near-conductive behaviour above 500 masl is represented well. The steeper conductive gradient below 500 masl is also matched very well with temperatures above 350^{o}C encountered below the foot of the well.

The supercritical model also significantly improves the match to the downhole temperatures in MW-04. With the current resolution the two shallow cold inflows are not captured in either model but the large, deep inflow is resolved by the supercritical model. Both models represent the main upflow area centred around MW-06 well. However, the bottom-hole temperature is beyond the range of the standard model and is only matched well by the supercritical version.

The match obtained for MW-08 by the standard model was quite poor. In comparison the supercritical model captures the conductive profile very well. As with the other wells a more refined supercritical model is required to match the sharp cold inflow at 1000 masl. Both models predict the temperatures in MW-09 poorly. As indicated in the diagrams it is located between MW-04 and MW-06 and despite this its downhole temperature profile differs dramatically from both. The data for this well needs to be reviewed and the model refined in this area to achieve a better match.

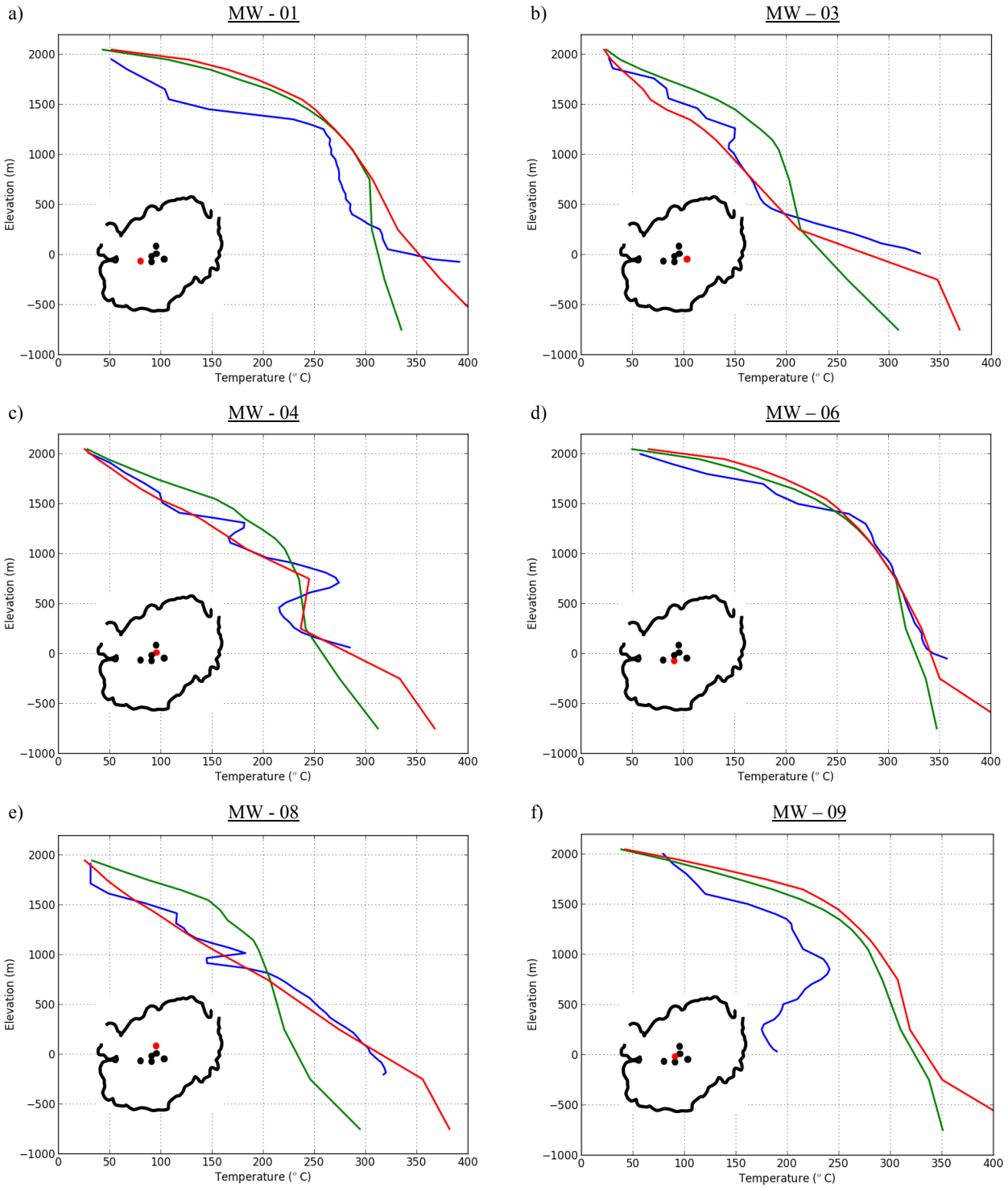

Figure 7: Downhole temperatures for six Menengai exploration wells. Measured data shown in blue, the supercritical model results in red, and the standard model results in green. Location of each well within the caldera also indicated with a red point.

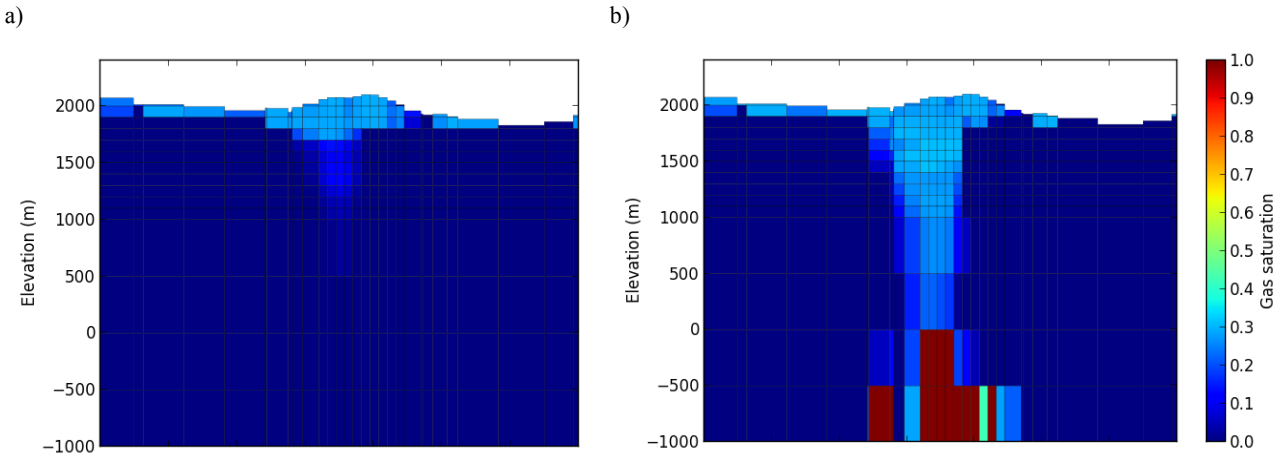

Figure 8: Predictions of natural state gas saturation on section A-A for (a) the standard model and (b) the supercritical model.

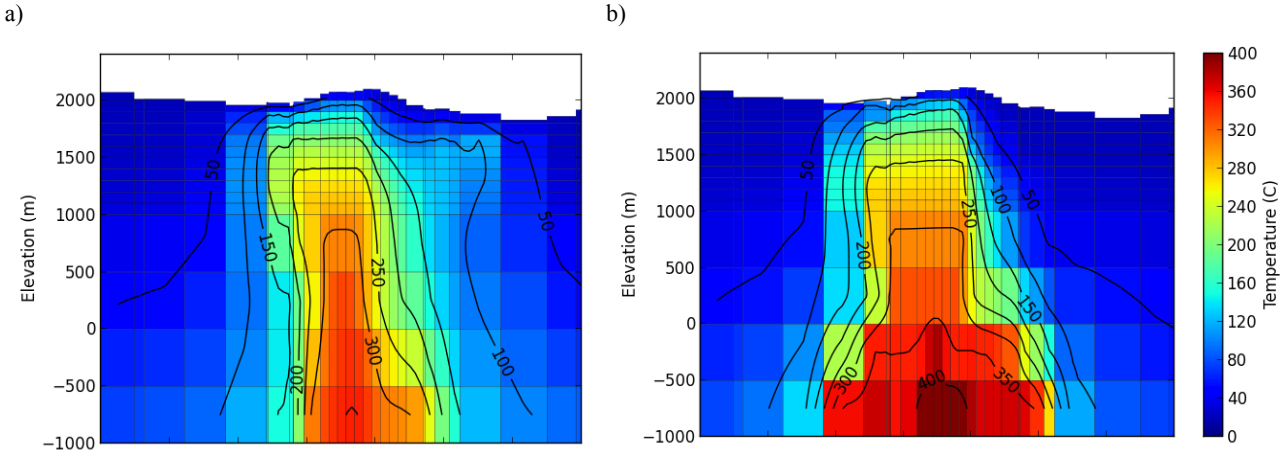

Figure 9: Predictions of natural state temperatures on section A-A for (a) the standard model and (b) the supercritical model.

The plots in Figures 8 and 9 show the differences in the gas saturation and temperatures on section A-A for the standard model and the supercritical model. Plot (b) in Figure 8 shows that the supercritical model predicts a steam zone extending from the water table all the way down to the supercritical fluid encountered at the bottom of the model. This agrees well with the available data which indicates that steam zones exist at elevations between 1000 to 1500 masl and 400 to 700 masl. In order match the separation between the steam zones further refinement of the model grid is required at these depths.

The temperature contours shown in Figure 9 reveal that the supercritical model not only provides a better match to the deep temperatures found in the Menengai system but also for the cold inflow from the east of the caldera that is found at shallow elevations. This is because the supercritical model is able to include the low vertical permeability that exists in the eastern part of the caldera between 0 masl and 500 masl and the high temperatures that it causes.

5. PRODUCTION SCENARIOS

Once the natural state model had been calibrated, three different production scenarios were run. These scenarios were based on the indicative scenarios that were run in our previous work in order to investigate the system's response to long term exploitation (Kipyego *et al.*, 2013). The scenarios are only indicative because at this stage there is only a very limited amount of production data and the schedule of development for the system is not yet certain. The scenarios were as follows:

Scenario 1	40 additional production wells added in three phases throughout Menengai caldera and Olrongai ridge
Scenario 2	Production wells added as in Scenario 1 with infield reinjection of approximately 20% of the total mass produced
Scenario 3	Production wells added as in Scenario 1 with outfield reinjection of approximately 20% of the total mass produced

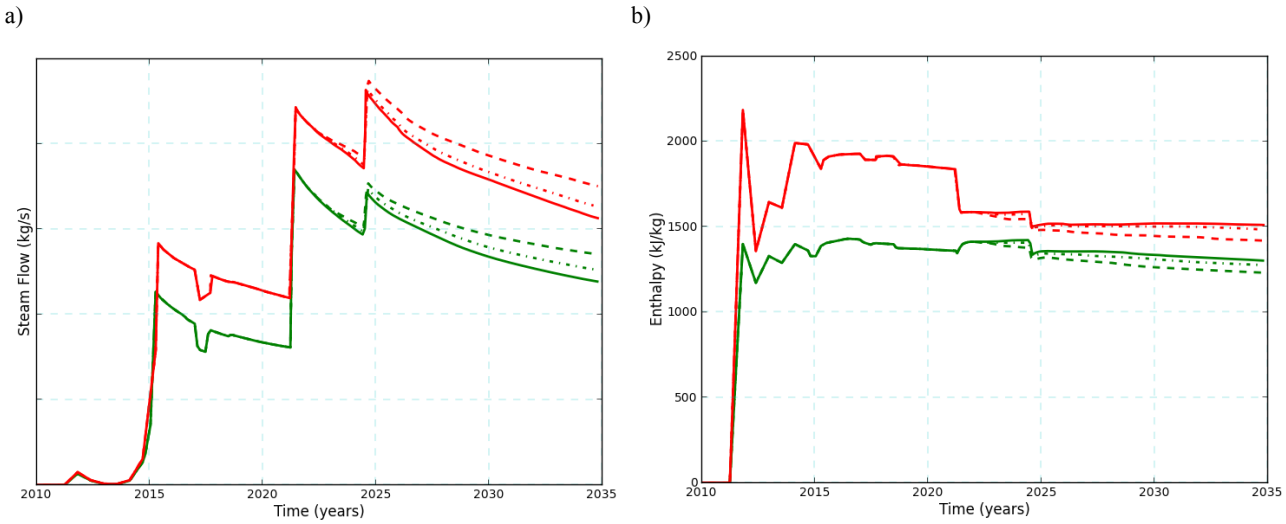

Figure 10: Predictions of steam flow (a) and average enthalpy (b) for three different production scenarios. The solid lines correspond to no reinjection, the dashed lines to infield reinjection and the dot-dashed lines to outfield reinjection. The results obtained using the standard model are shown in green and the supercritical model in red.

In both reinjection scenarios the fluid was re-injected with an enthalpy of 334.9 kJ/kg corresponding to 80°C and the re-injection was commenced in 2022, several years after production started, making a delayed re-injection strategy part of field development as suggested by Kaya and O'Sullivan (2010).

The results for the predicted steam flow for all three scenarios, using both the standard model and the supercritical model, are plotted in Figure 10 (a). The impact of accurately modelling the high temperatures found in the Menengai system is immediately apparent. Compared with the standard model the supercritical model predicts approximately 30% more steam from the same production scenario. The higher temperatures in the supercritical model mean that the average enthalpy is also predicted to be greater than in the standard model as shown in plot (b). Also, because of the higher heat flow in the supercritical model the average enthalpy of the fluid produced remains constant after 2025 for the no re-injection scenario whereas it continues to decay when using the standard model.

The effect of re-injection in both models is similar with infield re-injection providing the best pressure support and higher steam flow. Plot (a) in Figure 11 shows that in the supercritical model the impact of the infield re-injection is slightly more significant than in the standard model but plot (b) also shows that the average enthalpy declines faster as a result. This is due to the higher temperature rock in the supercritical model converting re-injected fluid into steam more effectively but also cooling more rapidly.

6. CONCLUSION

A supercritical version of the Menengai geothermal reservoir model has been developed and calibrated using the supercritical version of AUTOUGH2. The calibration required increasing the heat flow at the base of the model and adjusting some of the deep permeabilities. The model provides more accurate matches to the measured downhole temperature profiles than the previously published results obtained using the standard AUTOUGH2 simulator.

The supercritical model was then used to carry out three potential production scenarios and the results were compared with those obtained using the standard model. The results show that by accurately representing the high temperatures and supercritical conditions in the Menengai system, approximately 30% more steam is produced than is predicted by the standard model running the same scenario. Such a large difference in the predictions emphasises the need for modelling the high-temperature conditions in the system accurately and the continued development of supercritical modelling techniques.

REFERENCES

Croucher, A. E. and O'Sullivan, M. J.: Application of the computer code TOUGH2 to the simulation of supercritical conditions in geothermal systems, *Geothermics*, **37**, (2008), 622-634.

Lagat, J.: Geothermal surface exploration approach: case study of Menengai geothermal field, Kenya, *Proceedings*, Kenya Geothermal Conference, Kenyatta International Conference Centre, Nairobi, November 21-21, (2011).

Leat, P. T.: Geological Evolution of the Trachytic Caldera Volcano Menengai, Kenya rift Valley, *Journal of the Geological Society*, **141**, (1984), 1057-1069. doi:10.1144/gsjgs.141.6.1057.

Kaya, E., and O'Sullivan, M.: Modelling of Injection into Vapour-Dominated Geothermal systems, *Proceedings*, World Geothermal Congress, Bali, Indonesia (2010).

Kipyego, E., O'Sullivan, J. and O'Sullivan, M.: An initial resource assessment of the Menengai calder geothermal system using an air-water TOUGH2 model, Proceedings, 35th New Zealand Geothermal Workshop, Rotorua, November 18-20, (2013).

McCall, G. J. H.: Geology of the Nakuru-Thomson's Falls lake Hannington Area, Ministry of Natural Resources, Geological Survey of Kenya, (1967).

Mibei, G., and Lagat, J.: Structural Controls in Menengai Geothermal Field, *Proceedings* Kenya Geothermal Conference, Kenyatta International Conference Centre, Nairobi, November 21-21, (2011).

Omondi, C.: Borehole Geology and Hydrothermal Mineralisation of Wells MW-01 and MW-02, Menengai Geothermal Field, Central Kenya Rift Valley, Report 30, Orkustofnun, Grensasvegur 9, IS-108 Reykjavik, Iceland: United Nations university, (2011).

O'Sullivan, M. J., Pruess, K., and Lippmann, M. J.: State of the art of geothermal reservoir simulation, *Geothermics*, **30 (4)**, (2001), 395-429.

Pruess, K., Oldenburg, C., and Moridis, G.: TOUGH2 USER'S GUIDE, VERSION 2, Earth Sciences Division, Lawrence Berkeley National Laboratory: University of California, (1999).

Simiyu, S. M.: Application of Micro-Seismic Methods to Geothermal Exploration: Examples from the Kenya Rift, Short Course on Exploration for Geothermal Resources: UNU-GTP, KenGen and GDC, (2009).

Wheildon, J., Morgan, P., Williamson, K. H., Evans, T. R., and Swanberg, C. A.: Heat Flow in the Kenya Rift Zone, *Tectonopyhsics*, **236**, (1994), 131-149.

Yeh, A., Croucher, A. and O'Sullivan, M.J.: Recent developments in the AUTOUGH2 simulator, *Proceedings*, TOUGH Symposium, Berkeley, California, September 17-19, (2012).